Trivariate Analysis of Changes in Drought Characteristics in the CMIP6 Multimodel Ensemble at Global Warming Levels of 1.5°, 2°, and 3°C

HOSSEIN TABARI[a] AND PATRICK WILLEMS[a]

[a] *Department of Civil Engineering, KU Leuven, Leuven, Belgium*

(Manuscript received 24 December 2021, in final form 10 May 2022)

ABSTRACT: Drought is a major natural hazard with far-reaching social, economic, and environmental impacts whose characteristics are highly interdependent across different spatial and temporal scales. Traditional global warming impact assessments on drought at the global scale have, however, taken into account only one drought characteristic at a time, likely leading to an underestimation of the overall impact. Here, we perform a trivariate analysis of changes in drought conditions at 1.5°, 2°, and 3°C global warming levels using 25 CMIP6 GCMs. Drought properties are characterized by the Standardized Soil Moisture Index (SSI). The future joint return periods of droughts historically associated with 10-, 20-, and 30-yr return periods are computed under the warming levels using copula functions considering drought duration, peak, and severity. Our comparative assessments of global warming impact on drought properties between univariate and trivariate analyses corroborate the substantial underestimation of the impact by the univariate analysis. The trivariate analysis shows that around 63%–91% of the global land will be subject to more recurrent droughts, while the percentage of the land reduces to 41%–56% for the univariate analysis. The difference between the univariate and trivariate analyses enlarges with global warming levels and the extremity of drought events. Based on the trivariate analysis, a 30-yr drought would become at least threefold more recurrent in 11%, 15%, and 20% of the global land at 1.5°, 2°, and 3°C warming levels, respectively, but the univariate analysis could not reach such large increases in drought conditions.

KEYWORDS: Drought; Climate change; Statistical techniques; Soil moisture; Water resources

1. Introduction

Drought is one of the most destructive natural disasters due to its prolonged and extensive socioeconomic impacts (Carrão et al. 2016; Mukherjee et al. 2018). During the 1970–2019 period, drought was responsible for 34% of disaster-related fatalities in the world and 95% of disaster-related fatalities in Africa (WMO 2021). Due to inevitable global warming in the twenty-first century, the global water cycle has been intensifying (Hegerl et al. 2015), leading to more extreme events (Tabari 2020; Lange et al. 2020). Drought can be more severe and widespread under global warming through either decreasing precipitation and/or increasing evaporation (Dai 2011, 2013; Trenberth et al. 2014). Projected severe droughts would cause stress in water resources, threaten water security, and ultimately affect society (Hervás-Gámez and Delgado-Ramos 2020). Due to the far-reaching impacts of drought, its analysis under different global warming levels has received great attention from researchers (Sieck et al. 2021), especially after the Paris Climate Agreement that set a target to keep global warming well below 2°C compared to preindustrial times and aimed to limit it even further to 1.5°C (UNFCCC 2015). These Paris targets (i.e., 1.5° and 2°C) have become the focus of several global drought studies (Lehner et al. 2017; Liu et al. 2018; Betts et al. 2018; Xu et al. 2019; Gu et al. 2020; Wu et al. 2020).

The identification and characterization of drought is challenging because of its slow onset and recovery, lack of a unified definition, and the difficult specification of its exact area (Wilhite 2000). It becomes even more complex by the interdependencies between drought characteristics (e.g., between duration and severity). Owing to these interdependencies at different spatial and temporal scales, a univariate analysis may lead to a significant underestimation of the overall drought impact (Zscheischler and Seneviratne 2017). In other words, when different drought characteristics are simultaneously considered, an amplified climate change impact is expected. For example, in a univariate assessment, a moderate but long-lasting drought is barely considered as an extreme event, whereas it can quickly deplete stored water and consequently reduce resilience to subsequent droughts (Lehner et al. 2017). A multivariate analysis of drought characteristics is thus essential for a more realistic estimation of the climate change impact to design adequate adaptation strategies. However, most global studies on future climate change impacts on droughts have taken into account only one drought characteristic at a time (univariate analysis) (e.g., Liu et al. 2018; Xu et al. 2019; Spinoni et al. 2020; Liu et al. 2021), although several local and regional studies have characterized future drought changes based on a multivariate analysis (e.g., Madadgar and Moradkhani 2013; Afshar et al. 2020).

For a multivariate drought analysis, traditional methods require the same family of marginal distribution for drought characteristics, which might restrict their potential for practical applications (Shiau 2006; Song and Singh 2010). Copulas can overcome the identical marginal distribution limitation and enable the construction of a multivariate probability distribution

Denotes content that is immediately available upon publication as open access.

Supplemental information related to this paper is available at the Journals Online website: https://doi.org/10.1175/JCLI-D-21-0993.s1.

Corresponding author: Hossein Tabari, hossein.tabari@kuleuven.be

DOI: 10.1175/JCLI-D-21-0993.1

function for correlated variables that might not be best fitted by the same type of distribution (Shiau and Modarres 2009). Copula functions have shown promising results for a compound analysis between several single variables by solely focusing on modeling the dependence structure rather than marginal modeling (i.e., modeling the distribution of each separate variable), which is the case of multivariate models (Favre et al. 2004). In addition to the ability of copula functions to characterize the dependence structure independently of the type of marginal distributions, they allow a flexible mensuration of the tail dependence (Serinaldi et al. 2009) as well as the estimation of conditional probabilities (Ribeiro et al. 2019). They have, therefore, recently gained popularity for drought analysis (Xu et al. 2020; Yang et al. 2020; Jehanzaib et al. 2021; Wu et al. 2021; Poonia et al. 2021). Nevertheless, most of the previous studies using copula functions focus on the local scale, and comprehensive studies on a global scale are limited.

The handful of existing global studies of multivariate drought analysis under climate change (Gu et al. 2020; Wu et al. 2021) have characterized droughts using the Standardized Precipitation Index (SPI) and the Standardized Precipitation Evapotranspiration Index (SPEI). Drought quantification based on these indices is however potentially subject to biases. The SPI underestimates Earth's land drying trends by considering only water supply side changes (precipitation) and disregarding the interaction between land surface processes, atmospheric demand, and plants (Burke and Brown 2008; Vicente-Serrano et al. 2010). The SPEI overestimates drying trends by equally weighting both precipitation and potential (not actual) evapotranspiration. The offline estimation of potential evapotranspiration in SPEI also overpredicts the changes in non-water-stressed evapotranspiration calculated by climate models by neglecting stomatal conductance reductions induced by elevated atmospheric CO_2 (Milly and Dunne 2016). Global warming impacts on drought are therefore more meaningfully assessed by direct examination of climate model outputs (e.g., soil moisture and runoff) that more explicitly represent the core physical processes that are missing in the estimates of simple index-based impact models (e.g., SPI and SPEI) (Milly and Dunne 2016; Greve et al. 2019).

The previous global multivariate assessments of future droughts (Gu et al. 2020; Wu et al. 2021) used general circulation model (GCM) simulations from phase 5 of the Coupled Model Intercomparison Project (CMIP5), which consider only emission scenarios in the form of four representative concentration pathways (RCPs). In the state-of-the-art CMIP6 simulations (Eyring et al. 2016), the climate projections not only are produced by updated climate models but also include a wider range of forcing than CMIP5 by considering socioeconomic scenarios based on the Shared Socioeconomic Pathways (SSPs) next to the RCPs (O'Neill et al. 2016). For the former, the simulations of the CMIP6 GCMs are expected to better represent physical processes at smaller scales (Stouffer et al. 2017) such as an improved process of interactions between the world's two major climate phenomena: El Niño–Southern Oscillation (ENSO) and the Indian Ocean dipole (IOD) (McKenna et al. 2020). For the latter, the inclusion of SSPs complements the RCPs and then makes future scenarios more reasonable (NCC Editorial Staff 2019). In addition, a larger number of simulations for the same forcing in the CMIP6 dataset enables a better representation of internal variabilities (Pascoe et al. 2019; Merrifield et al. 2020).

To address the aforementioned shortcomings, this study aims to quantify changes in global droughts using a trivariate copula analysis. In addition to 1.5° and 2°C targets of the Paris Climate Agreement, we also analyze the changes at a higher warming level of 3°C, which provides new insights for drought impact under far future conditions and highlights the consequence of failure to meet the global warming targets. We determine the global warming levels of 1.5°, 2°, and 3°C by the time sampling method (Vautard et al. 2014) where specific time periods in the future are identified when the global mean temperature increase in a GCM reaches a certain level. Drought is characterized at three time scales (3, 6, and 12 months) by the Standardized Soil Moisture Index (SSI) using simulations from 25 CMIP6 GCMs. A trivariate analysis is then performed to assess the joint impact of global warming on drought characteristics (duration, peak, and severity) by the best-fitted copula function, and the changes in the trivariate return period of drought under the three global warming levels are quantified.

2. Materials and methods

a. Data

We used the climate data from the CMIP6 GCMs, covering the entire historical (1850–2014) and future (2015–2100) periods under four CMIP6 Tier 1 SSP scenarios, including SSP1-2.6, SSP2-4.5, SSP3-7.0, and SSP5-8.5. SSP1-2.6, SSP2-4.5, and SSP5-8.5 can be seen as continuations of the RCP2.6, RCP4.5, and RCP8.5 scenarios from CMIP5 respectively, while SSP3-7.0 presents a new scenario with high-level emissions (O'Neill et al. 2016). This set of scenarios covers a wide range of uncertainties in future greenhouse gas forcings coupled to the corresponding socioeconomic developments. Of the CMIP6 GCMs, 25 models (Table S1 in the online supplemental material) have monthly simulations for near-surface air temperature and total soil moisture content for the selected SSP scenarios from 1850 to 2100. The mean temperature is used to calculate global warming levels above the preindustrial period and soil moisture as an input for drought quantification using SSI.

b. Estimation of global warming

The warming is referred to as an increase in multidecadal global mean surface temperature (GMST) above preindustrial levels representing a climate without anthropogenic influence. In this study, the preindustrial temperature is defined as the GMST of the 30-yr period 1850–79. Three global warming levels of 1.5°, 2°, and 3°C are determined by the time sampling method (Vautard et al. 2014). The warming is computed by subtracting the preindustrial temperature from the running mean of 30-yr GMST over the entire period. To account for different sensitivities of climate models, the first 30-yr periods of global warming reaching 1.5°, 2°, and 3°C under different SSP scenarios versus the preindustrial temperature are determined for each model.

c. Drought characterization

We characterize drought using a multi-time-scalar indicator to assess changes in drought conditions for the future, which allows tailoring the drought impact for different sectors such as water resources, agriculture, forestry, and ecology (Beguería et al. 2014). A multiscalar feature is essential for drought studies owing to the highly varying arrival periods of water inputs to usable water resources (Vicente-Serrano et al. 2010). We employ the SSI (Hao and AghaKouchak 2013), whose computation follows the SPI (McKee et al. 1993) calculation procedure, but with soil moisture as input instead of precipitation. The SSI is calculated in this study at the 3-, 6-, and 12-month scales (SSI-3, SSI-6, and SSI-12), representing the degree of wetness/dryness over different time periods. The empirical Gringorten plotting position is employed to compute the empirical probability for soil moisture data [$P = (i - 0.44)/(n + 0.12)$, where n is the length of the data and i is the rank]. The SSI values are computed by standardizing the empirical probability by the inverse normal transformation (Farahmand and AghaKouchak 2015).

After computing the SSI time series (1850–2100) for each model grid cell at the global scale, the run theory is employed to detect drought events. We define that a drought event starts when the SSI value is less than -0.5 (X_0), lasts when the value ($X_{i,t}$) stays less than -0.5 for at least three consecutive months (including the first starting month), and ends when the indicator is greater than -0.5. The threshold of -0.5 is chosen to ensure sufficient number of events per 30-yr period for a more reliable estimation of the parameters of marginal distributions and copulas as in previous studies (Hao and AghaKouchak 2014; Gu et al. 2020). A sensitivity analysis is performed to test the sensitivity of the results to the selected threshold for defining a drought event. The independence between events is maximized by setting an independence period (at least three months) between two events. The drought characteristics are defined as follows (Fig. S1): drought duration (DD) as the number of months of a drought event, drought frequency (DF) as the number of drought events in a given period, and drought peak (DP) as the maximum of the absolute values of the SSI in a recognized drought event; drought severity (DS) as the absolute sum value of the SSI through a given event. Moreover, the interarrival time (DI) is estimated as the period from the beginning of one event to the beginning of the next event (Shiau and Shen 2001). To compute the ensemble median of the GCMs, drought statistics are regridded at a spatial resolution of 2.0° × 2.0°. The error of this last-step procedure is less than a first-step procedure in which data are first resampled, and then climate change signals are computed (Diaconescu et al. 2015).

d. Trivariate distribution analysis

To analyze the complex nature of drought and discover the compound effect of three drought properties (duration, peak, and severity), copula functions are employed in this study. A copula function can couple different marginal distributions and present the joint probability distribution. The function can be written as

$$H(x_1, x_2, x_3, \ldots, x_m) = C[F_1(x_1), F_2(x_2), F_3(x_3), \ldots, F_m(x_m)] = C(u_1, u_2, u_3, \ldots, u_m), \quad (1)$$

where H represents an m-dimensional distribution function of random variables (x_1, x_2, x_3, … , x_m), C is a copula function: $[0, 1]^2 \rightarrow [0, 1]$, ($F_1$, F_2, F_3, … , F_m) are one-dimensional marginal cumulative distribution functions, and (u_1, u_2, u_3, … ,u_m) are variables produced by marginal distribution functions [$F_1(x_1)$, $F_2(x_2)$, $F_3(x_3)$, … , $F_m(x_m)$] in the unit interval [0, 1].

Copula functions are usually limited to two-dimensional analysis because it is difficult to construct them in higher dimensions (Kao and Govindaraju 2008). To overcome this difficulty and allow us to use copulas for higher-dimensional analysis, one solution is to couple bivariate copulas to construct higher-dimensional copulas (Grimaldi and Serinaldi 2006). A trivariate copula can accordingly be constructed based on a modified bivariate copula expressed as

$$C(u_1, u_2, u_3) = C_2[C_1(u_1, u_2), u_3], \quad (2)$$

where C_1 is the first bivariate copula function corresponding to variables u_1 and u_2 and C_2 is the second bivariate copula function corresponding to variables $C_1(u_1, u_2)$ and u_3. The C_1 and C_2 are the same type of copula functions.

e. Selection of the best-fitted marginal and copula functions

To conduct a copula analysis, the best-fitted one-dimensional distribution function for each drought property should be determined. The three drought properties are fitted to 16 marginal distributions (Birnbaum-Saunders, exponential, extreme value, gamma, generalized extreme value, generalized Pareto, inverse Gaussian, logistic, loglogistic, lognormal, Nakagami, normal, Rayleigh, Rician, t location scale, Weibull), and then the best-fitted distribution is determined based on the Bayesian information criterion (BIC). After determining the most representative marginal distribution for each property, the best-fitted copula function between different properties needs to be identified. In contrast to most previous studies that have employed only one copula family (Tosunoglu and Can 2016; Gu et al. 2020), we test the goodness of fit of seven copula functions (Gaussian, Clayton, Frank, Gumbel, Ali-Mikhail-Haq, Joe, and Plackett) from three families (Archimedean, elliptical, and Plackett) (Table S2) to find the best one for further analyses. The parameters of these copulas are estimated using the maximum likelihood method (ML). To avoid the misleading performance assessment of copula functions with a single measure (Sadegh et al. 2017), an ensemble of measures is employed including root-mean-square error (RMSE), Nash-Sutcliff efficiency (NSE), Akaike information criterion (AIC), and BIC.

f. Estimation of joint return periods

To examine the composite impact of global warming on drought characteristics, the trivariate joint return period (JRP) is computed as

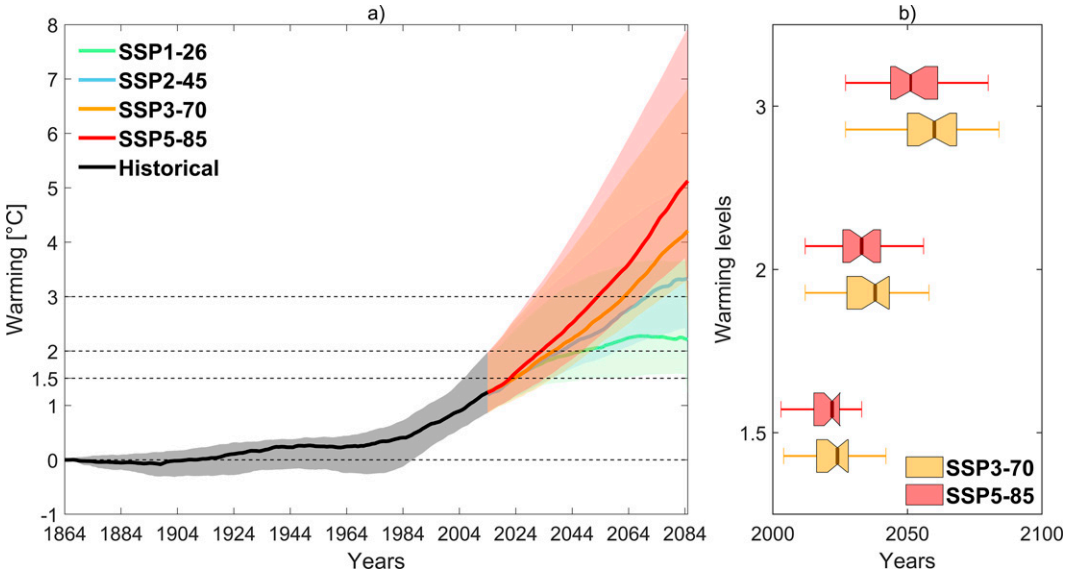

FIG. 1. (a) Global warming relative to the preindustrial (1850–79) mean for 25 CMIP6 GCMs and (b) GCM-wide distributions of the years for different global warming levels. In (a), lines and uncertainty bands represent the ensemble median and interquartile range, respectively; the gray shaded area displays the range of historical simulations and the colored areas display the range of future global warming projections based on different SSP scenarios; the three global warming levels selected for this study are shown with dashed lines. In (b), the left and right of the box show the 75th and 25th percentiles of uncertainty range, respectively; the left and right of the whiskers show the 95th and 5th percentiles, respectively; and the vertical red line in the middle of the box represents the ensemble median.

$$T_{DPS} = \frac{E(L)}{P(D \geq d \text{ or } P \geq p \text{ or } S \geq s)} = \frac{E(L)}{1 - F_{DPS}(d,p,s)} = \frac{E(L)}{1 - C[F_D(d), F_P(p), F_S(s)]}, \quad (3)$$

where T_{DPS} denotes the JRP for drought when duration (D) or peak (P) or severity (S) are equal to or greater than certain duration (d) and peak (p) and severity (s) values, respectively, and where $E(L)$ is the drought interarrival period for the corresponding level (30 years). The term F_{DPS} represents joint cumulative distribution function (CDF) of the three properties (d, p, s) and can be presented as the product of a copula function (C) of three separate marginal CDFs (F_D, F_P, F_S) of the corresponding properties. The 10-, 20- and 30-yr JRPs are calculated in this study. With the historical quantiles of reference return periods, the JRP can be calculated for the future periods under different global warming levels considered here. Take a drought with a 10-yr return period as a case. We first identify the historical magnitudes of duration, peak, and severity for a 10-yr drought. Then, we use these magnitudes as inputs for the future marginal distribution function of properties under global warming levels. With the products of marginal distributions, the trivariate joint return period of 10-yr drought under each warming level is obtained through a trivariate copula. The future joint return period can be computed in another way where the joint return periods are obtained from the properties of historical droughts, and then the recurrence time of this historical joint return period under future climatic conditions is derived. Our results show that the future joint return periods computed using these two methodologies do not differ in magnitude and global pattern for most cases (Fig. 7; see also Fig. S8). We thus present only the results of the first methodology in this paper. Because the first methodology is far less computationally demanding, its use is also recommended for future studies.

g. *Trivariate correlation analysis*

The copula is constructed on the correlated variables, and thus it is essential to examine the magnitude and significance of the correlation. Unlike past trivariate studies that only tested correlations between every two variables, we introduce the multiple correlation coefficient (R) to analyze the correlations between the three variables. The R is always used to assess the relationship between one dependent variable (predictand) and a combination of other independent variables (predictors). Thus, three variables of this study can be sorted into three orders with the form y–$x1$–$x2$: DS–DD–DP, DP–DS–DD, and DD–DP–DS. The multiple correlation coefficient can be written as

$$R = \sqrt{\frac{R_{x1y}^2 + R_{x2y}^2 - 2R_{x1y}R_{x2y}R_{x1x2}}{1 - R_{x1x2}^2}}, \quad (4)$$

where R is the multiple correlation coefficient, R_{x1y} is the bivariate correlation coefficient between predictor $x1$ and predictand y, R_{x2y} is the bivariate correlation coefficient between predictor $x2$ and predictand y, and R_{x1x2} is the bivariate correlation coefficient between the two predictors $x1$ and $x2$ (Cohen et al. 2003).

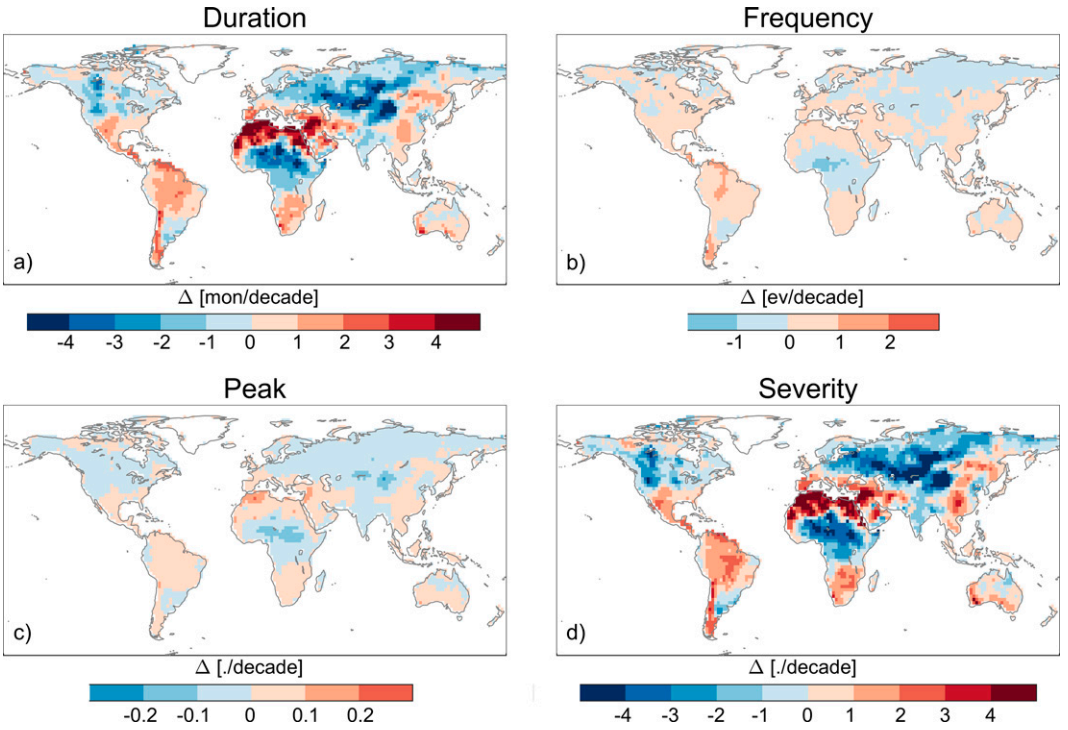

FIG. 2. Projected changes in drought characteristics derived from SSI-12 for 1.5°C warming level based on the ensemble median of 25 CMIP6 GCMs.

The Student's *t* test is used for statistical significance testing of the correlation for different orders of the three variables.

3. Results

a. Estimation of global warming

The median and interquartile range of the estimated global warming for the historical period and the future period under different SSP scenarios are illustrated in Fig. 1a. As expected, the magnitude of global warming increases with the SSP scenario. The projections of global warming based on SSPs start to diverge in 2030, as emissions start to slow down in SS1-2.6 and continue as usual in SSP5-8.5. For the 30-yr period at the end of this century (2071–2100), the ensemble median of warming for each scenario is as follows: 2.2°C for SSP1-2.6, 3.3°C for SSP2-4.5, 4.3°C for SSP3-7.0, and 5.1°C for SSP5-8.5. Under the SSP5-8.5 scenario, the median global warming across GCMs reaches 1.5°, 2°, and 3°C warming in the 2020s, 2030s, and 2050s, respectively (Fig. 1b). Compared to SSP5-8.5, the three global warming levels will be reached later under the SSP3-7.0 scenario as expected. Only a few GCMs can reach 2°C under SSP1-2.6 and 3°C under SSP2-4.5. Because this research aims to study drought under three global warming levels of 1.5°, 2°, and 3°C, SSP1-2.6 and SSP2-4.5 were excluded from the analyses. In addition, the results for the drought characteristics for the three global warming levels show a negligible difference between SSP3-7.0 and SSP5-8.5. We thus only discuss the results for the SSP5-8.5-derived global warming levels.

b. Univariate analysis of drought properties under global warming

After estimating global warming levels, the expected changes in drought properties compared to the preindustrial levels are quantified under different warming levels. The univariate analysis of drought properties shows an uneven spatial pattern of the changes, with the largest increases in South America, central America, the Middle East and North Africa (MENA), southern Europe, southern Africa, Australia, and parts of eastern Asia (Figs. 2–4). While the spatial distribution of the changes remains almost the same with global warming levels, the absolute magnitude of the changes increases with warming. The increasing signals for different global warming levels are found over 42%–45%, 44%–56%, 41%–44%, and 42%–44% of the global land for duration, frequency, peak, and severity, respectively. The absolute magnitudes of the changes per decade respectively for 1.5°, 2°, and 3°C warming levels are 0.86, 1.01, and 1.23 days for duration; 0.21, 0.24, and 0.3 for frequency; 0.032, 0.037, and 0.044 for peak; and 1.18, 1.41, and 1.71 for severity. While the spatial distribution of changes in drought properties is similar across all the time scales of SSI, the magnitude becomes smaller from SSI-12 to SSI-3 (Figs. S2 and S3).

The changes in drought properties under different global warming levels compared to the preindustrial levels are further examined in the six most impacted subcontinental regions (central America, eastern North America, the Mediterranean, Amazon, southern Africa, and Australia). The results for the 12-month scale are shown in Fig. 5. For all six regions, drought

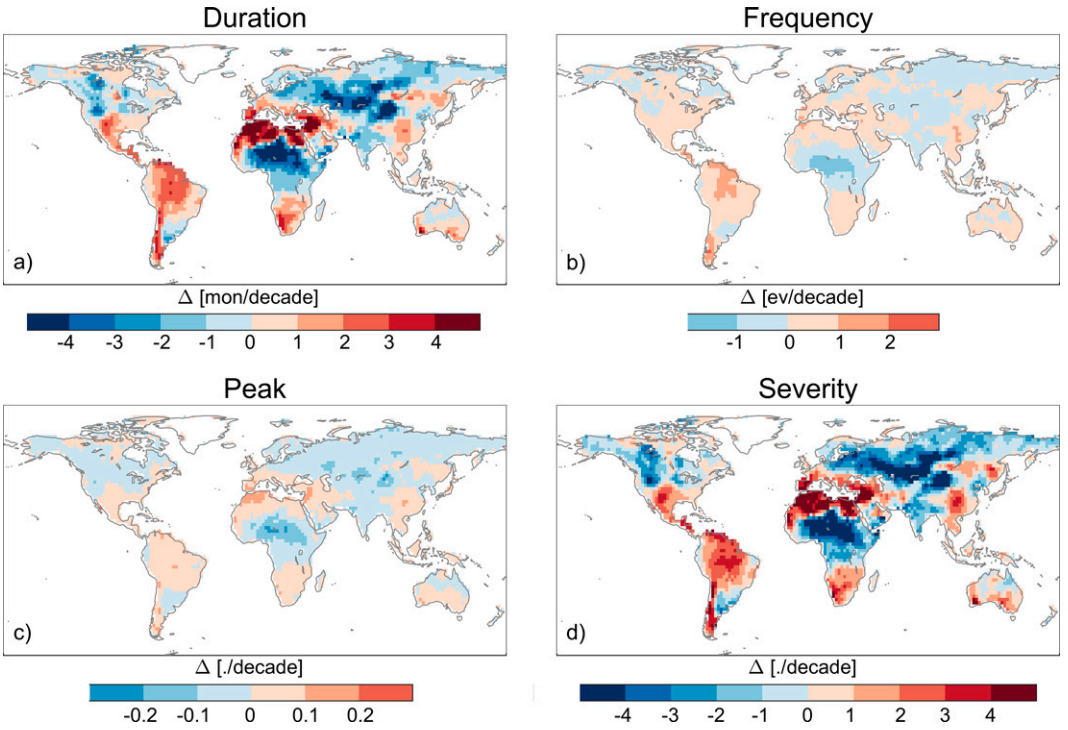

FIG. 3. Projected changes in drought characteristics derived from SSI-12 for 2°C warming level based on the ensemble median of 25 CMIP6 GCMs.

properties in order of increasing change magnitude are peak, frequency, duration, and severity. The magnitude of the increasing signal for all properties is largest in the Mediterranean followed by the Amazon and Central America. The duration, peak, and severity of droughts rise with global warming levels in all six regions, whereas there is no clear pattern for frequency. For different global warming levels, the change differences between 2° and 3°C levels are notably larger than those between 1.5° and 2°C levels, as expected. In a 3°C warming world, the magnitudes of the increases in duration, peak, and severity in the Mediterranean is respectively 2.6, 3, and 3.2 times larger than those at 1.5°C warming level and 1.7, 1.7, and 1.8 times larger than those at 2°C warming level. Similar factors are found in the Amazon and Central America by comparing the increasing magnitude of duration, peak, and severity across the three global warming levels. The uncertainty analysis of the changes indicates that the larger the change, the larger the GCM uncertainty. This pattern holds for both drought properties and regions; the largest GCM uncertainty is found for severity among drought properties and in the Mediterranean among the six most impacted regions. For all drought properties, the GCM uncertainty increase with lead time is consistent with previous studies (Lehner et al. 2020; Zhou et al. 2020).

In the six regions, the longer the time scale is, the larger the changes in duration, peak, and severity are (Fig. S4). This pattern is not followed by drought frequency except in southern Africa. Taking a 3°C warming over Amazon as an example, the median changes at the 12-month scale for duration, peak, and severity are 56%, 25%, and 85% respectively, while they are 39%, 16%, and 59% for the respective properties at the 3-month scale. We also checked the sensitivity of the results to the choice of threshold for defining drought events. The results show similar global patterns and magnitude of changes in drought properties across different thresholds (Fig. S5).

c. *Trivariate analysis of drought properties under global warming*

The multiple correlation coefficient (R) was applied to test the relationship between drought duration, peak, and severity. The range of the R values for all GCMs over the entire 1850–2100 period for three orders of the drought properties (DS–DD–DP, DP–DS–DD, and DD–DP–DS) is presented in Fig. 6. The results indicate high and significant (p value < 0.05) correlations among properties, with the median coefficient > 0.9 for all orders of the drought properties. The coefficients for different orders of the properties are of comparable magnitude. With a slight difference, they are ordered in terms of magnitude as DS–DD–DP, DD–DP–DS, and DP–DS–DD. The highest correlation is obtained when severity is considered as the predictand because of a high correlation of severity with both duration and peak. In contrast, owing to a lower predictability of extremes (peak), considering peak as the predictand results in the lowest correlation.

After the correlation examination, the goodness of fit of 16 marginal distributions for drought properties is evaluated. The percentage of the global land area with the best-fitted distributions for the three drought properties is shown in Fig. 7. The generalized Pareto distribution (GPD) is the dominant marginal distribution for drought peak and duration and

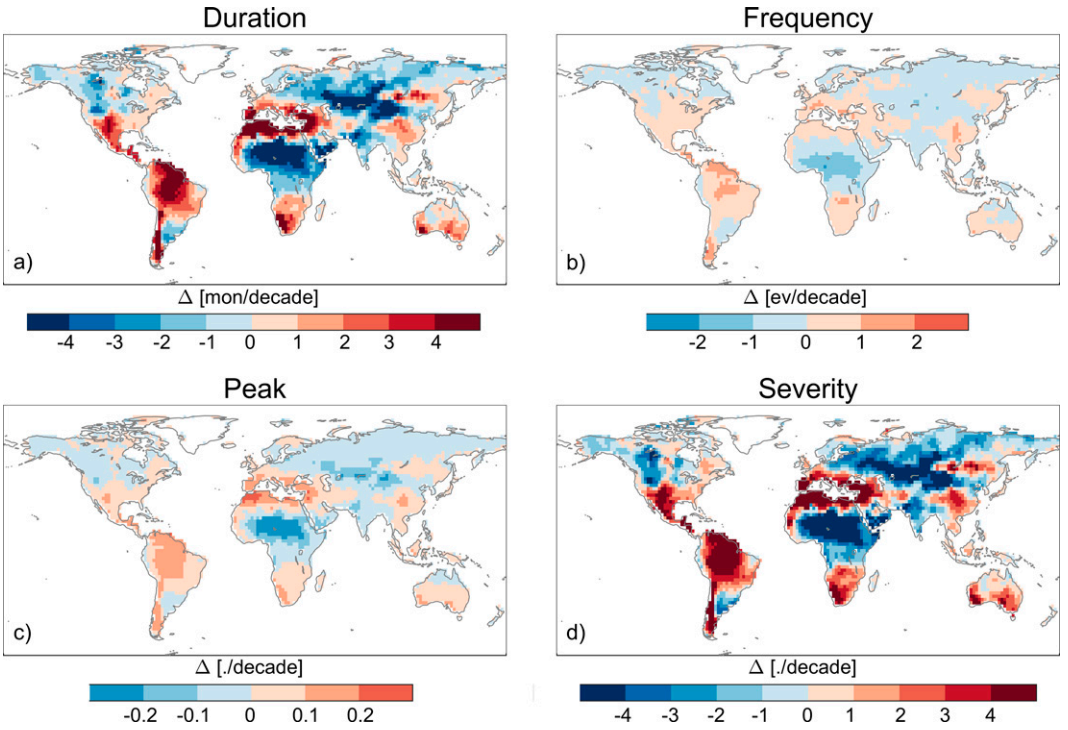

FIG. 4. Projected changes in drought characteristics derived from SSI-12 for 3°C warming level based on the ensemble median of 25 CMIP6 GCMs.

the third-best distribution for severity, although the difference between the top three distributions for severity is small (3.5%). The exponential distribution, which is among the top three distributions for severity, can be considered as a limiting case of the three-parameter GPD when the shape parameter, describing the tail behavior of the distribution, is equal to zero. The best-fitted distributions for severity, ranging from bounded to heavy-tailed distributions, show diverse statistical behaviors of drought severity across the globe. In contrast, the peak can be best approximated by the GPD across almost the entire global land, varying between 80% and 95% of the global land depending on climate models. It indicates a uniform global distribution of drought peak. The good performance of the GPD for peak is expected as it is a heavy-tailed distribution suitable for approximating extreme values as previously shown for other types of meteorologically related extremes (Katz et al. 2002; Hosseinzadehtalaei et al. 2020). Due to a strong linkage between duration and severity, the distribution of duration follows that of severity, which is a varying statically behavior across the globe, although the GPD (the best-fitted distribution over 27% of the global land) is much better than the other distributions. Owing to a good performance of the GPD, it is selected as the theoretical distribution of the three properties.

After selecting the marginal distribution for the drought properties, the next step is to choose the best copula function for the joint distribution analysis between the properties. To this end, the performance of seven copula functions (Gaussian, Clayton, Frank, Gumbel, Ali-Mikhail-Haq, Joe, and Plackett) is evaluated compared to the empirical joint distribution. Figure 8 presents the land percentage of the best-fitted copula functions for all CMIP6 GCMs. The best-fitted copula function for a grid cell is selected if it performs best based on at least three out of the four performance measures (RMSE, NSE, AIC, and BIC). Among the tested copula functions, Joe, Gaussian, and Frank copulas are the top three copulas that perform best for most grid cells. Joe is the best-fitted copula over 28%–54% of the global land, depending on GCMs.

The seven selected copulas account for either only positive dependence between variables (e.g., Joe) or both positive and negative dependencies (e.g., Frank). Since drought duration, severity, and peak have a strong positive dependence, the difference between the performances of the copulas cannot be due to the sign of correlations between the variables. The discrepancy between the performances of the copulas is then related to the role of the tail behavior of severity, duration, and peak. The best performance of the Joe function from the Archimedean family of copulas is because it can reproduce well the upper tail dependence structure (i.e., a higher association for large values) across the three drought properties (Ribeiro et al. 2020). In contrast, the weak performance of the Clayton copula from the same family is due to the fact that the dependence of the three variables in the upper tail of this copula is very weak (Lee et al. 2013).

The joint return periods of droughts in the future under different global warming levels historically associated with return periods of 10, 20, and 30 years derived from the Joe copula are shown in Figs. 9–11. The results show that the recurrence of droughts will increase in most of the global land area under

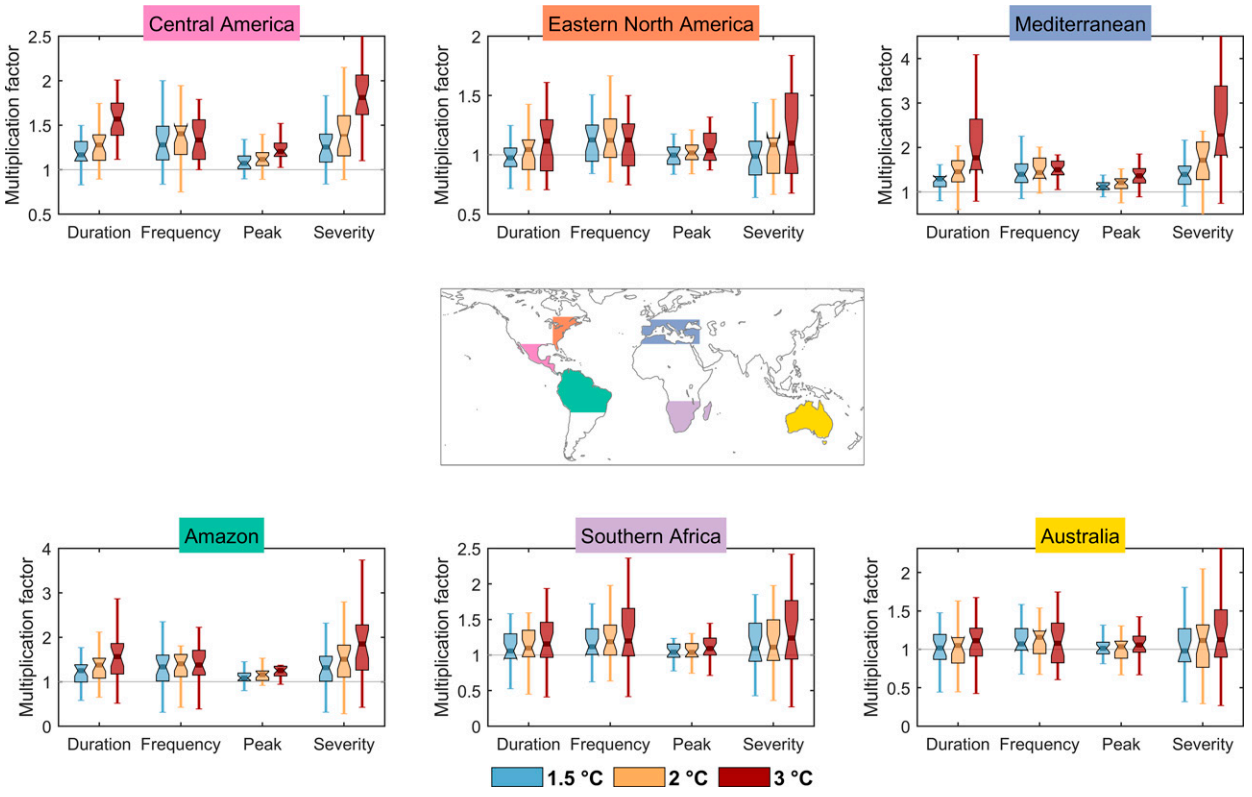

FIG. 5. Projected changes in drought properties derived from SSI-12 under different global warming levels for the six most impacted regions. The multiplication factor is the ratio of future drought properties over the historical ones. The top and bottom of the boxes show the 75th and 25th percentiles of uncertainty range, respectively; the top and bottom of the whiskers show the 95th and 5th percentiles, respectively; and the horizontal red line in the middle of the box represents the ensemble median.

global warming. Around 63%–91% of the global land, depending on return periods and warming levels, will be subject to more recurrent droughts, while the univariate analysis leads to a less widespread increase in drought properties: increasing signals over 41%–56% of the land area depending on drought properties and warming levels. The percentage of the global land area exposed to a higher drought recurrence increases with the global warming level. The impact of global warming also increases with the rarity of drought events. The longer the return period, the larger the change in the drought recurrence. About 1%, 9%, and 11% of the global land with at least threefold increase in the recurrence of 10-, 20-, and 30-yr droughts under 1.5°C warming expand to 1%, 14%, and 15% under 2°C warming, and 2%, 19%, and 20% under 3°C warming.

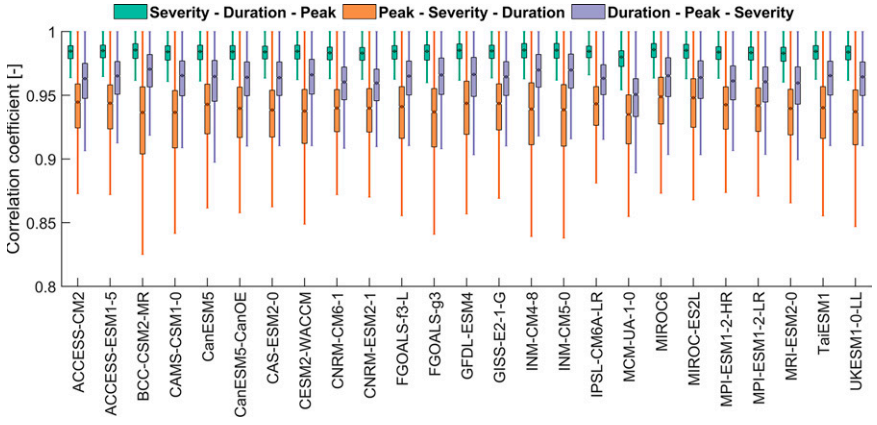

FIG. 6. Multiple correlation coefficients between drought properties for all CMIP6 GCMs.

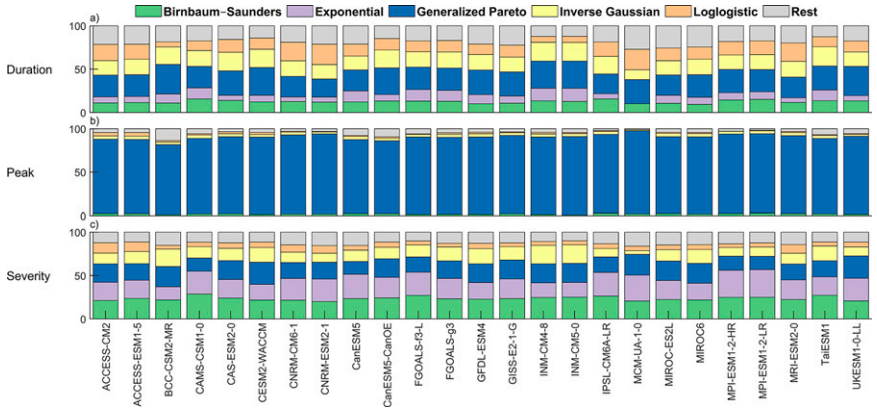

FIG. 7. Percentage of the global land area of the best-fitted marginal distributions for different drought properties for all CMIP6 GCMs. "Rest" refers to the rest of distribution functions.

Similar to the univariate analysis, the results of the trivariate analysis of drought are further examined in the six most impacted regions (Fig. 12). The increase of change magnitudes with the drought event extremity and global warming levels is obvious in the plots (Fig. 12). Our trivariate analysis identifies the Amazon as the most impacted region where 30-yr droughts will be 3, 4.1, and 4.2 times more recurrent under 1.5°, 2°, and 3°C global warming, respectively. The factors for the respective warming levels in Amazon are 2.6, 3.3, and 4 for 20-yr droughts and 1.8, 2, and 2.1 for 10-yr droughts. For 30-yr droughts, we find 2.2–3.9 fold increases in the drought recurrence for the Mediterranean, 2.5–3.4 for southern Africa, 2.3–3.4 for Central America, 1.7–2.6 for eastern North America, and 1.5–1.7 in Australia, depending on warming levels. A comparison between the results of univariate and trivariate analyses for the six most impacted regions reveals that the univariate analysis leads to much smaller drought changes under global warming (Figs. 5 and 12).

In addition to the six hotspot regions identified by the univariate analysis, eastern Africa and eastern Asia are also severely impacted based on the results of the trivariate analysis where twice more recurrent droughts are expected. We also performed the trivariate analysis using the Gaussian function as the second-best copula (Figs. S6 and S7). The Gaussian copula produces a similar joint probability and a similar spatial pattern of changes. The magnitude of the changes is however slightly larger for the Gaussian copula compared to the Joe copula.

4. Discussion

Our trivariate analysis of drought properties reveals that the percentage of the global land area exposed to an increase in drought recurrence escalates with global warming levels. At least a threefold increase in the recurrence of 10-, 20-, and 30-yr droughts under 1.5°C warming is expected in 1%, 9%, and 11% of the global land respectively, which enlarge to 1%, 14%, and 15% under 2°C warming, and 2%, 19%, and 20% under 3°C warming. It suggests that the impact of global warming increases with the extremity of drought events. Larger impacts of climate change on more severe hydroclimatic extreme events have also been previously reported (Kharin et al. 2018; Hosseinzadehtalaei

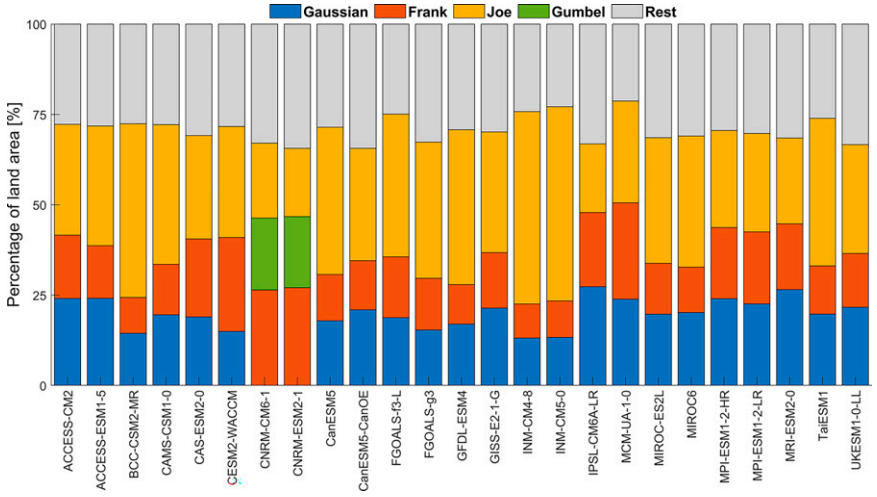

FIG. 8. Percentage of the global land area of the best-fitted copula functions for different CMIP6 GCMs. "Rest" refers to the rest of the copula functions.

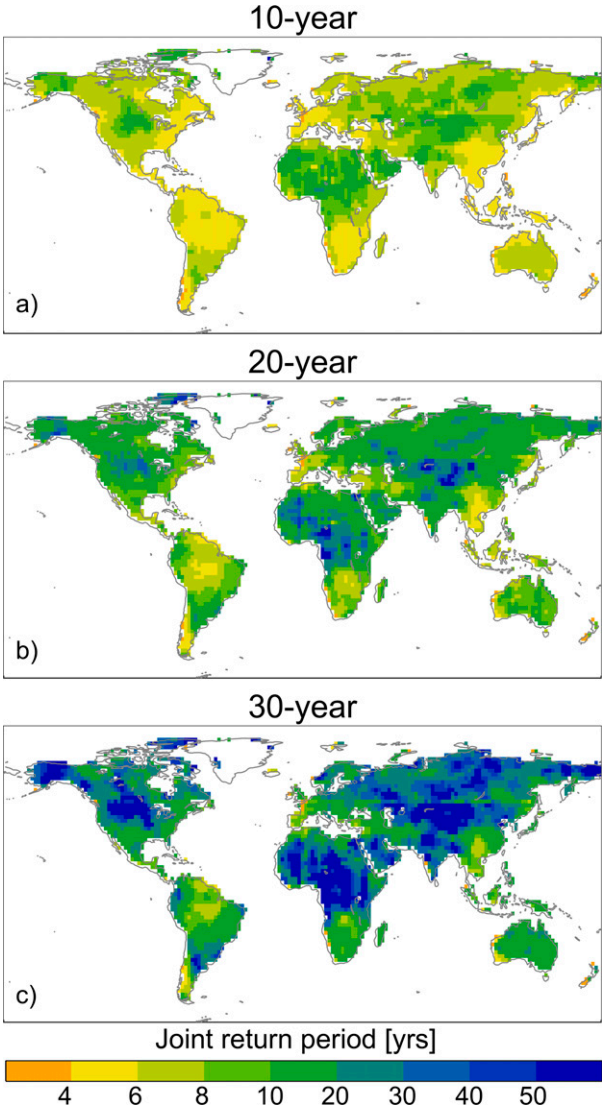

FIG. 9. Joint return periods of droughts historically associated with return periods of 10, 20, and 30 years in the future under 1.5°C global warming level using the Joe copula function.

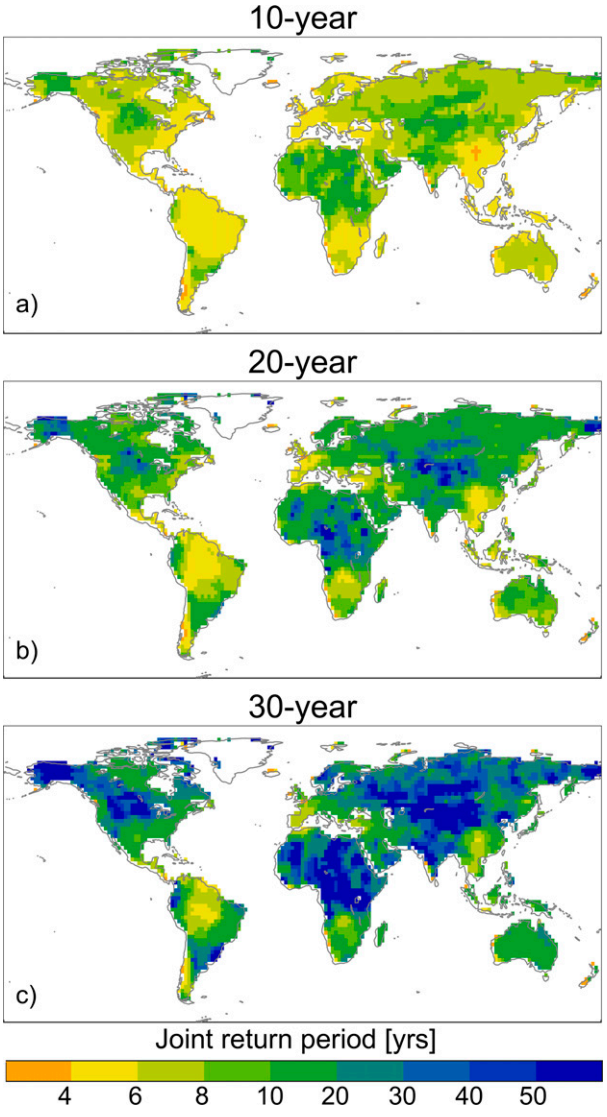

FIG. 10. Joint return periods of droughts historically associated with return periods of 10, 20, and 30 years in the future under 2°C global warming level using the Joe copula function.

et al. 2019; Li et al. 2019; Tabari 2021). A comparison between the results of univariate and trivariate analyses of drought under global warming approves the assumption that a univariate analysis would underestimate the impact. Our results show that the 30-yr droughts are expected to become more recurrent in 63%–91% of the land area, depending upon return periods and warming levels. The univariate analysis projects smaller and less widespread changes for drought characteristics under global warming. These findings are insightful in the sense that a univariate analysis not only underestimates extreme events in the current climate, which was reported in previous studies (e.g., Gräler et al. 2013; Sadegh et al. 2018; Nikraftar et al. 2021), but also the impact of global warming on extreme events. In other words, the bias in the estimation of extreme events for both historical and future climates by a univariate analysis is not compensated in relative changes (under global warming levels) but is propagated. Our results show that a univariate analysis may not reveal a significant relationship between drought characteristics and represent an accurate picture of future global warming impacts on droughts. In fact, drought events of a higher peak and severity often last longer (Ji et al. 2022), leading to an accumulated overall impact that is overlooked in a univariate framework. Such incapability of the univariate analysis was previously shown for comprehensively describing historical regional drought events (Ayantobo et al. 2018). The results of this study also reveal a strong positive relationship between drought characteristics across the globe. These strong positive relationships are not spatially and temporally uniform, because of some exceptional occurrences of slowly evolving drought events with low peaks (Ayantobo et al. 2019) or a rapid intensification over a short

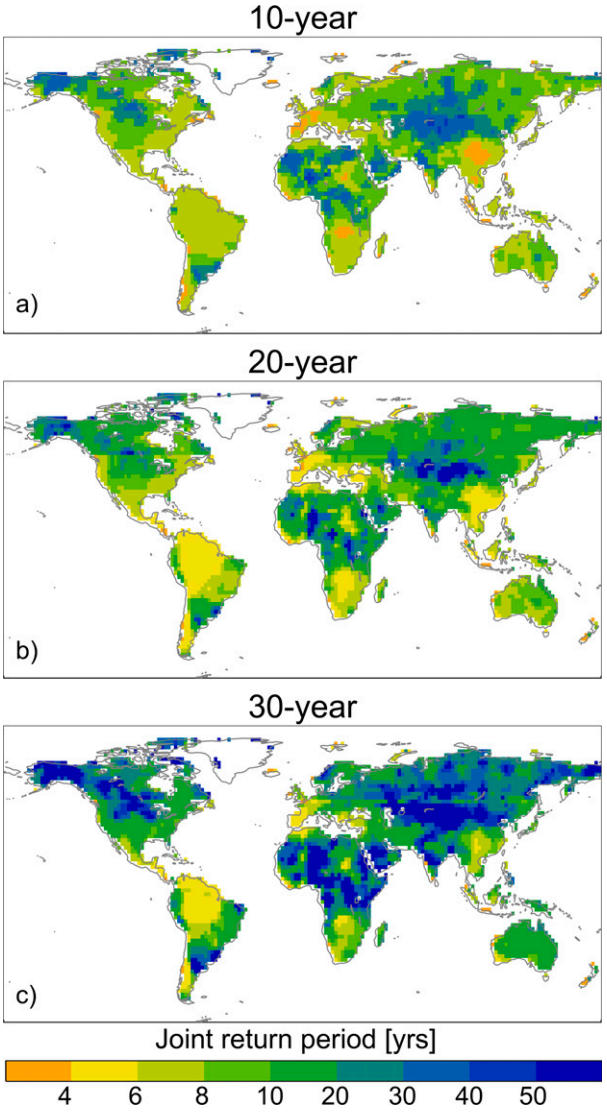

FIG. 11. Joint return periods of droughts historically associated with return periods of 10, 20, and 30 years in the future under 3°C global warming level using the Joe copula function.

period of time (Christian et al. 2019). A multivariate analysis using copulas allows a better understanding of these relationships for more reliable drought projections.

Our results also reveal that the increase in drought recurrence with global warming is not spatially uniform and a greater magnitude of the increase is expected for the Americas (especially Central America, eastern North America, and the Amazon), southern and eastern Africa, the Mediterranean, Australia, and eastern Asia. In fact, wherever both water demand component increase and water supply decrease happen, the decrease in water availability would be remarkable (Tabari et al. 2021), which is the case more for arid regions of the world or for other regions with high water stress due to population density and high water demand. Specifically, the increment of evapotranspiration under global warming (1.5%–4% per degree of warming; Scheff and Frierson 2014) can decrease the remainder of water for the land when precipitation cannot compensate for the extra evaporation. Our results also show that these drought conditions adopt a prolonged pattern under global warming, particularly in arid regions. That will increase the already high level of water stress in these regions and force people to migrate or live in conditions of water poverty and eventually raise the risk of political conflict over transboundary water resources (Tabari and Willems 2018).

The projected strong increases in drought conditions will harm crop production and degrade food security especially in regions that are highly dependent on climate-sensitive agriculture specially rain-fed cereals. The United States, China, Brazil, and Argentina are respectively the world's biggest corn producers (U.S. Department of Agriculture 2021) that will experience a remarkably higher recurrence of droughts, leading to global food insecurity and huge damages. For example, the 2003 European summer drought in combination with heatwave caused an extensive crop deficit in parts of southern Europe of a total cost of approximately 15 billion euros (García-Herrera et al. 2010). A more reliable projection of drought impacts can form the basis of proactive planning to limit such damages in the future.

5. Conclusions

The impact of global warming on drought at the global scale was scrutinized in this study by a trivariate copula-based analysis at 1.5°, 2°, and 3°C warming levels. Drought characteristics at the 3-, 6-, and 12-month scales were identified by SSI based on the climate simulations from 25 CMIP6 GCMs. The joint return periods of droughts historically associated with return periods of 10, 20, and 30 years were determined for the future under different global warming levels. The univariate drought analysis identifies central America, eastern North America, the Mediterranean, Amazon, southern Africa, and Australia as hotspot regions. In addition to these regions, Africa and eastern Asia are recognized as severely impacted regions by the trivariate analysis where drought recurrence will be doubled. The duration, peak, and severity of droughts rise with global warming levels in all hotspot regions, whereas there is no clear pattern for frequency. Similarly, the percentage of the global land area exposed to a higher drought recurrence in the trivariate framework increases with the global warming level. For both analyses, the longer the time scale is, the larger the changes in drought conditions are. Compared to the univariate analysis, the trivariate analysis however demonstrates larger changes in drought conditions. Around 1%, 9%, and 11% of the land area would be exposed to 3 times more recurrent 10-, 20-, and 30-yr droughts under 1.5°C global warming. The drought conditions would worsen with higher global warming levels, where the percentages for the respective return periods grow to 1%, 14%, and 15% for 2°C warming level, and 2%, 19%, and 20% for 3°C warming level. In the Mediterranean and Amazon, fourfold more recurrent droughts are expected under global warming. A univariate analysis could not reach such a large increase in drought conditions. The results underscore the need of using a multivariate drought analysis considering the interdependency between different characteristics as

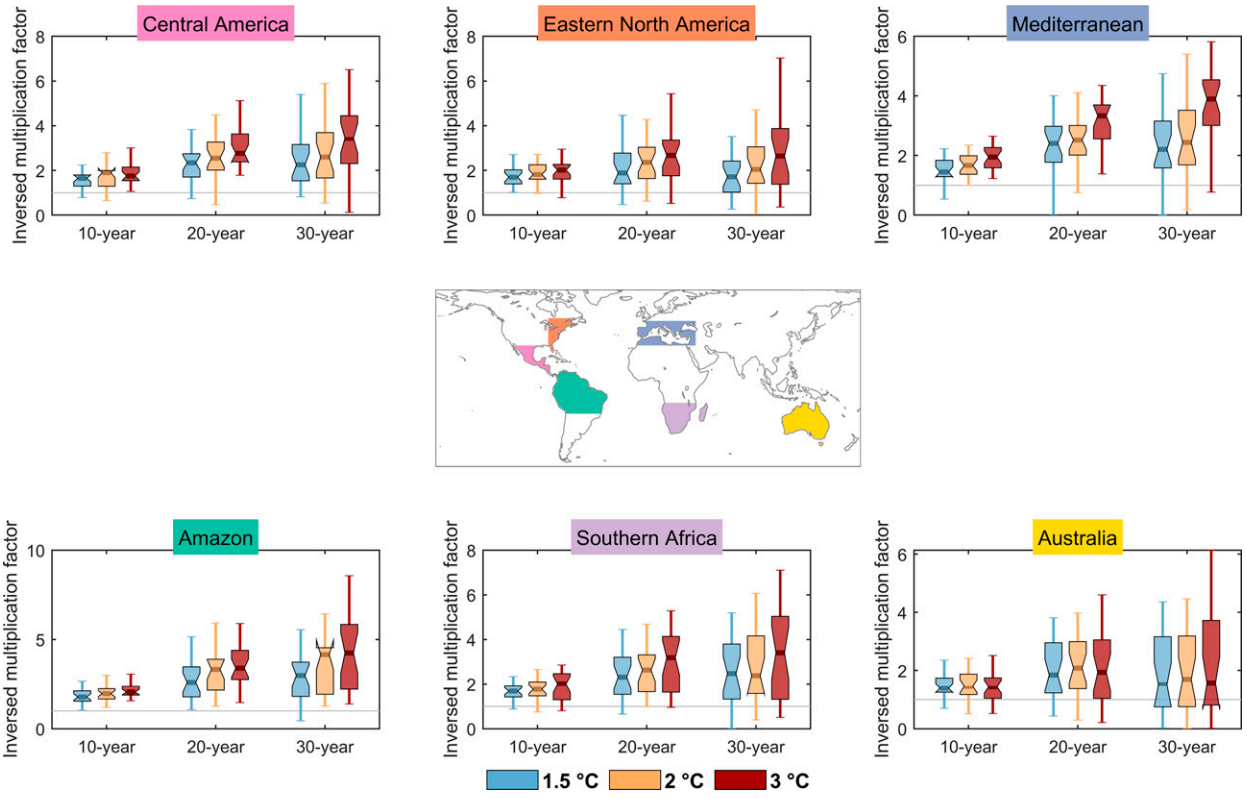

FIG. 12. Projected changes in the joint return periods of droughts historically associated with return periods of 10, 20, and 30 years in the future under different global warming levels for the six most impacted regions using the Joe copula function. The multiplication factor was inversed for an easier comparison between the results of univariate and trivariate analyses. The top and bottom of the box show the 75th and 25th percentiles of uncertainty range, respectively; the top and bottom of the whiskers show the 95th and 5th percentiles, respectively; the horizontal red line in the middle of the box represents the ensemble median.

otherwise the impact of global warming on drought may be underestimated.

Acknowledgments. This research was supported by funding from the Research Foundation–Flanders (FWO) (Grant 12P3222N). We would also like to thank climate modeling centers for developing the CMIP6 GCMs and making their outputs available. We have no conflict of interest to declare.

Data availability statement. The CMIP6 mean temperature and soil moisture data used in this study can be accessed online through the Earth System Grid Federation (ESGF) system.

REFERENCES

Afshar, M. H., A. Ü. Şorman, F. Tosunoğlu, B. Bulut, M. T. Yilmaz, and A. Danandeh Mehr, 2020: Climate change impact assessment on mild and extreme drought events using copulas over Ankara, Turkey. *Theor. Appl. Climatol.*, **141**, 1045–1055, https://doi.org/10.1007/s00704-020-03257-6.

Ayantobo, O. O., Y. Li, S. Song, T. Javed, and N. Yao, 2018: Probabilistic modelling of drought events in China via 2-dimensional joint copula. *J. Hydrol.*, **559**, 373–391, https://doi.org/10.1016/j.jhydrol.2018.02.022.

——, ——, and ——, 2019: Copula-based trivariate drought frequency analysis approach in seven climatic sub-regions of mainland China over 1961–2013. *Theor. Appl. Climatol.*, **137**, 2217–2237, https://doi.org/10.1007/s00704-018-2724-x.

Beguería, S., S. M. Vicente-Serrano, F. Reig, and B. Latorre, 2014: Standardized precipitation evapotranspiration index (SPEI) revisited: Parameter fitting, evapotranspiration models, tools, datasets and drought monitoring. *Int. J. Climatol.*, **34**, 3001–3023, https://doi.org/10.1002/joc.3887.

Betts, R. A., and Coauthors, 2018: Changes in climate extremes, fresh water availability and vulnerability to food insecurity projected at 1.5°C and 2°C global warming with a higher-resolution global climate model. *Philos. Trans. Roy. Soc.*, **A376**, 20160452, https://doi.org/10.1098/rsta.2016.0452.

Burke, E. J., and S. J. Brown, 2008: Evaluating uncertainties in the projection of future drought. *J. Hydrometeor.*, **9**, 292–299, https://doi.org/10.1175/2007JHM929.1.

Carrão, H., G. Naumann, and P. Barbosa, 2016: Mapping global patterns of drought risk: An empirical framework based on sub-national estimates of hazard, exposure and vulnerability. *Global Environ. Change*, **39**, 108–124, https://doi.org/10.1016/j.gloenvcha.2016.04.012.

Christian, J. I., J. B. Basara, J. A. Otkin, E. D. Hunt, R. A. Wakefield, P. X. Flanagan, and X. Xiao, 2019: A methodology for flash drought identification: Application of flash

drought frequency across the United States. *J. Hydrometeor.*, **20**, 833–846, https://doi.org/10.1175/JHM-D-18-0198.1.

Cohen, J., P. Cohen, S. G. West, and L. S. Aiken, 2003: *Applied Multiple Regression/Correlation Analysis for the Behavioral Sciences.* 3rd ed., Lawrence Erlbaum Associates Publishers, 703 pp.

Dai, A., 2011: Drought under global warming: A review. *Wiley Interdiscip. Rev.: Climate Change*, **2**, 45–65, https://doi.org/10.1002/wcc.81.

——, 2013: Increasing drought under global warming in observations and models. *Nat. Climate*, **3**, 52–58, https://doi.org/10.1038/nclimate1633.

Diaconescu, E. P., P. Gachon, and R. Laprise, 2015: On the remapping procedure of daily precipitation statistics and indices used in regional climate model evaluation. *J. Hydrometeor.*, **16**, 2301–2310, https://doi.org/10.1175/JHM-D-15-0025.1.

Eyring, V., S. Bony, G. A. Meehl, C. A. Senior, B. Stevens, R. J. Stouffer, and K. E. Taylor, 2016: Overview of the Coupled Model Intercomparison Project Phase 6 (CMIP6) experimental design and organization. *Geosci. Model Dev.*, **9**, 1937–1958, https://doi.org/10.5194/gmd-9-1937-2016.

Farahmand, A., and A. AghaKouchak, 2015: A generalized framework for deriving nonparametric standardized drought indicators. *Adv. Water Resour.*, **76**, 140–145, https://doi.org/10.1016/j.advwatres.2014.11.012.

Favre, A. C., S. El Adlouni, L. Perreault, N. Thiémonge, and B. Bobée, 2004: Multivariate hydrological frequency analysis using copulas. *Water Resour. Res.*, **40**, W01101, https://doi.org/10.1029/2003WR002456.

García-Herrera, R., J. Díaz, R. M. Trigo, J. Luterbacher, and E. M. Fischer, 2010: A review of the European summer heat wave of 2003. *Crit. Rev. Environ. Sci. Technol.*, **40**, 267–306, https://doi.org/10.1080/10643380802238137.

Gräler, B., M. J. van den Berg, S. Vandenberghe, A. Petroselli, S. B. D. Grimaldi, B. De Baets, and N. E. C. Verhoest, 2013: Multivariate return periods in hydrology: A critical and practical review focusing on synthetic design hydrograph estimation. *Hydrol. Earth Syst. Sci.*, **17**, 1281–1296, https://doi.org/10.5194/hess-17-1281-2013.

Greve, P., M. L. Roderick, A. M. Ukkola, and Y. Wada, 2019: The aridity index under global warming. *Environ. Res. Lett.*, **14**, 124006, https://doi.org/10.1088/1748-9326/ab5046.

Grimaldi, S., and F. Serinaldi, 2006: Asymmetric copula in multivariate flood frequency analysis. *Adv. Water Resour.*, **29**, 1155–1167, https://doi.org/10.1016/j.advwatres.2005.09.005.

Gu, L., and Coauthors, 2020: Projected increases in magnitude and socioeconomic exposure of global droughts in 1.5° and 2°C warmer climates. *Hydrol. Earth Syst. Sci.*, **24**, 451–472, https://doi.org/10.5194/hess-24-451-2020.

Hao, Z., and A. AghaKouchak, 2013: Multivariate standardized drought index: A parametric multi-index model. *Adv. Water Resour.*, **57**, 12–18, https://doi.org/10.1016/j.advwatres.2013.03.009.

——, and ——, 2014: A nonparametric multivariate multi-index drought monitoring framework. *J. Hydrometeor.*, **15**, 89–101, https://doi.org/10.1175/JHM-D-12-0160.1.

Hegerl, G. C., and Coauthors, 2015: Challenges in quantifying changes in the global water cycle. *Bull. Amer. Meteor. Soc.*, **96**, 1097–1115, https://doi.org/10.1175/BAMS-D-13-00212.1.

Hervás-Gámez, C., and F. Delgado-Ramos, 2020: Are the modern drought management plans modern enough? The Guadalquivir River Basin Case in Spain. *Water*, **12**, 49, https://doi.org/10.3390/w12010049.

Hosseinzadehtalaei, P., H. Tabari, and P. Willems, 2019: Regionalization of anthropogenically forced changes in 3 hourly extreme precipitation over Europe. *Environ. Res. Lett.*, **14**, 124031, https://doi.org/10.1088/1748-9326/ab5638.

——, ——, and ——, 2020: Climate change impact on short-duration extreme precipitation and intensity–duration–frequency curves over Europe. *J. Hydrol.*, **590**, 125249, https://doi.org/10.1016/j.jhydrol.2020.125249.

Jehanzaib, M., J. Yoo, H. H. Kwon, and T. W. Kim, 2021: Reassessing the frequency and severity of meteorological drought considering non-stationarity and copula-based bivariate probability. *J. Hydrol.*, **603**, 126948, https://doi.org/10.1016/j.jhydrol.2021.126948.

Ji, Y., and Coauthors, 2022: Multivariate global agricultural drought frequency analysis using kernel density estimation. *Ecol. Eng.*, **177**, 106550, https://doi.org/10.1016/j.ecoleng.2022.106550.

Kao, S. C., and R. S. Govindaraju, 2008: Trivariate statistical analysis of extreme rainfall events via the Plackett family of copulas. *Water Resour. Res.*, **44**, W02415, https://doi.org/10.1029/2007WR006261.

Katz, R. W., M. B. Parlange, and P. Naveau, 2002: Statistics of extremes in hydrology. *Adv. Water Resour.*, **25**, 1287–1304, https://doi.org/10.1016/S0309-1708(02)00056-8.

Kharin, V. V., G. M. Flato, X. Zhang, N. P. Gillett, F. Zwiers, and K. J. Anderson, 2018: Risks from climate extremes change differently from 1.5°C to 2.0°C depending on rarity. *Earth's Future*, **6**, 704–715, https://doi.org/10.1002/2018EF000813.

Lange, S., and Coauthors, 2020: Projecting exposure to extreme climate impact events across six event categories and three spatial scales. *Earth's Future*, **8**, e2020EF001616, https://doi.org/10.1029/2020EF001616.

Lee, T., R. Modarres, and T. B. Ouarda, 2013: Data-based analysis of bivariate copula tail dependence for drought duration and severity. *Hydrol. Processes*, **27**, 1454–1463, https://doi.org/10.1002/hyp.9233.

Lehner, F., S. Coats, T. F. Stocker, A. G. Pendergrass, B. M. Sanderson, C. C. Raible, and J. E. Smerdon, 2017: Projected drought risk in 1.5°C and 2°C warmer climates. *Geophys. Res. Lett.*, **44**, 7419–7428, https://doi.org/10.1002/2017GL074117.

——, and Coauthors, 2020: Partitioning climate projection uncertainty with multiple large ensembles and CMIP5/6. *Earth Syst. Dyn.*, **11**, 491–508, https://doi.org/10.5194/esd-11-491-2020.

Li, C., and Coauthors, 2019: Larger increases in more extreme local precipitation events as climate warms. *Geophys. Res. Lett.*, **46**, 6885–6891, https://doi.org/10.1029/2019GL082908.

Liu, C., C. Yang, Q. Yang, and J. Wang, 2021: Spatiotemporal drought analysis by the standardized precipitation index (SPI) and standardized precipitation evapotranspiration index (SPEI) in Sichuan Province, China. *Sci. Rep.*, **11**, 1280, https://doi.org/10.1038/s41598-020-80527-3.

Liu, W., F. Sun, W. H. Lim, J. Zhang, H. Wang, H. Shiogama, and Y. Zhang, 2018: Global drought and severe drought-affected populations in 1.5° and 2°C warmer worlds. *Earth Syst. Dyn.*, **9**, 267–283, https://doi.org/10.5194/esd-9-267-2018.

Madadgar, S., and H. Moradkhani, 2013: Drought analysis under climate change using copula. *J. Hydrol. Eng.*, **18**, 746–759, https://doi.org/10.1061/(ASCE)HE.1943-5584.0000532.

McKee, T. B., N. J. Doesken, and J. Kleist, 1993: The relationship of drought frequency and duration to time scales. *Proc. Eighth Conf. on Applied Climatology*, Amer. Meteor. Soc., 179–183.

McKenna, S., A. Santoso, A. Sen Gupta, A. S. Taschetto, and W. Cai, 2020: Indian Ocean Dipole in CMIP5 and CMIP6: Characteristics, biases, and links to ENSO. *Sci. Rep.*, **10**, 11500, https://doi.org/10.1038/s41598-020-68268-9.

Merrifield, A. L., L. Brunner, R. Lorenz, I. Medhaug, and R. Knutti, 2020: An investigation of weighting schemes suitable for incorporating large ensembles into multi-model ensembles. *Earth Syst. Dyn.*, **11**, 807–834, https://doi.org/10.5194/esd-11-807-2020.

Milly, P. C., and K. A. Dunne, 2016: Potential evapotranspiration and continental drying. *Nat. Climate*, **6**, 946–949, https://doi.org/10.1038/nclimate3046.

Mukherjee, S., A. Mishra, and K. E. Trenberth, 2018: Climate change and drought: A perspective on drought indices. *Curr. Climate Change Rep.*, **4**, 145–163, https://doi.org/10.1007/s40641-018-0098-x.

NCC Editorial Staff, 2019: The CMIP6 landscape. *Nat. Climate Change*, **9**, 727, https://doi.org/10.1038/s41558-019-0599-1.

Nikraftar, Z., A. Mostafaie, M. Sadegh, J. H. Afkueieh, and B. Pradhan, 2021: Multi-type assessment of global droughts and teleconnections. *Wea. Climate Extremes*, **34**, 100402, https://doi.org/10.1016/j.wace.2021.100402.

O'Neill, B. C., and Coauthors, 2016: The Scenario Model Intercomparison Project (ScenarioMIP) for CMIP6. *Geosci. Model Dev.*, **9**, 3461–3482, https://doi.org/10.5194/gmd-9-3461-2016.

Pascoe, C., B. N. Lawrence, E. Guilyardi, M. Juckes, and K. E. Taylor, 2019: Designing and documenting experiments in CMIP6. *Geosci. Model Dev. Discuss.*, https://doi.org/10.5194/gmd-2019-98.

Poonia, V., S. Jha, and M. K. Goyal, 2021: Copula based analysis of meteorological, hydrological and agricultural drought characteristics across Indian river basins. *Int. J. Climatol.*, **41**, 4637–4652, https://doi.org/10.1002/joc.7091.

Ribeiro, A. F., A. Russo, C. M. Gouveia, and P. Páscoa, 2019: Copula-based agricultural drought risk of rainfed cropping systems. *Agric. Water Manage.*, **223**, 105689, https://doi.org/10.1016/j.agwat.2019.105689.

——, ——, ——, and C. A. Pires, 2020: Drought-related hot summers: A joint probability analysis in the Iberian Peninsula. *Wea. Climate Extremes*, **30**, 100279, https://doi.org/10.1016/j.wace.2020.100279.

Sadegh, M., E. Ragno, and A. AghaKouchak, 2017: Multivariate Copula Analysis Toolbox (MvCAT): Describing dependence and underlying uncertainty using a Bayesian framework. *Water Resour. Res.*, **53**, 5166–5183, https://doi.org/10.1002/2016WR020242.

——, and Coauthors, 2018: Multihazard scenarios for analysis of compound extreme events. *Geophys. Res. Lett.*, **45**, 5470–5480, https://doi.org/10.1029/2018GL077317.

Scheff, J., and D. M. Frierson, 2014: Scaling potential evapotranspiration with greenhouse warming. *J. Climate*, **27**, 1539–1558, https://doi.org/10.1175/JCLI-D-13-00233.1.

Serinaldi, F., B. Bonaccorso, A. Cancelliere, and S. Grimaldi, 2009: Probabilistic characterization of drought properties through copulas. *Phys. Chem. Earth*, **34**, 596–605, https://doi.org/10.1016/j.pce.2008.09.004.

Shiau, J. T., 2006: Fitting drought duration and severity with two-dimensional copulas. *Water Resour. Manage.*, **20**, 795–815, https://doi.org/10.1007/s11269-005-9008-9.

——, and H. W. Shen, 2001: Recurrence analysis of hydrologic droughts of differing severity. *J. Water Resour. Plann. Manage.*, **127**, 30–40, https://doi.org/10.1061/(ASCE)0733-9496(2001)127:1(30).

——, and R. Modarres, 2009: Copula-based drought severity–duration–frequency analysis in Iran. *Meteor. Appl.*, **16**, 481–489, https://doi.org/10.1002/met.145.

Sieck, K., C. Nam, L. M. Bouwer, D. Rechid, and D. Jacob, 2021: Weather extremes over Europe under 1.5° and 2.0°C global warming from HAPPI regional climate ensemble simulations. *Earth Syst. Dyn.*, **12**, 457–468, https://doi.org/10.5194/esd-12-457-2021.

Song, S., and V. P. Singh, 2010: Frequency analysis of droughts using the Plackett copula and parameter estimation by genetic algorithm. *Stochastic Environ. Res. Risk Assess.*, **24**, 783–805, https://doi.org/10.1007/s00477-010-0364-5.

Spinoni, J., and Coauthors, 2020: Future global meteorological drought hot spots: A study based on CORDEX data. *J. Climate*, **33**, 3635–3661, https://doi.org/10.1175/JCLI-D-19-0084.1.

Stouffer, R. J., V. Eyring, G. A. Meehl, S. Bony, C. Senior, B. Stevens, and K. E. Taylor, 2017: CMIP5 scientific gaps and recommendations for CMIP6. *Bull. Amer. Meteor. Soc.*, **98**, 95–105, https://doi.org/10.1175/BAMS-D-15-00013.1.

Tabari, H., 2020: Climate change impact on flood and extreme precipitation increases with water availability. *Sci. Rep.*, **10**, 13768, https://doi.org/10.1038/s41598-020-70816-2.

——, 2021: Extreme value analysis dilemma for climate change impact assessment on global flood and extreme precipitation. *J. Hydrol.*, **593**, 125932, https://doi.org/10.1016/j.jhydrol.2020.125932.

——, and P. Willems, 2018: More prolonged droughts by the end of the century in the Middle East. *Environ. Res. Lett.*, **13**, 104005, https://doi.org/10.1088/1748-9326/aae09c.

——, P. Hosseinzadehtalaei, W. Thiery, and P. Willems, 2021: Amplified drought and flood risk under future socioeconomic and climatic change. *Earth's Future*, **9**, e2021EF002295, https://doi.org/10.1029/2021EF002295.

Tosunoglu, F., and I. Can, 2016: Application of copulas for regional bivariate frequency analysis of meteorological droughts in Turkey. *Nat. Hazards*, **82**, 1457–1477, https://doi.org/10.1007/s11069-016-2253-9.

Trenberth, K. E., A. Dai, G. van der Schrier, P. D. Jones, J. Barichivich, K. R. Briffa, and J. Sheffield, 2014: Global warming and changes in drought. *Nat. Climate*, **4**, 17–22, https://doi.org/10.1038/nclimate2067.

UNFCCC, 2015: Paris Agreement. United Nations Framework Convention on Climate Change. Accessed 10 October 2021, https://unfccc.int/files/essential_background/convention/application/pdf/english_paris_agreement.pdf.

U.S. Department of Agriculture, 2021: World agricultural production. Accessed 10 December 2021, https://usda.library.cornell.edu/concern/publications/5q47rn72z?locale=en.

Vautard, R., and Coauthors, 2014: The European climate under a 2°C global warming. *Environ. Res. Lett.*, **9**, 034006, https://doi.org/10.1088/1748-9326/9/3/034006.

Vicente-Serrano, S. M., S. Beguería, and J. I. López-Moreno, 2010: A multiscalar drought index sensitive to global warming: The standardized precipitation evapotranspiration index. *J. Climate*, **23**, 1696–1718, https://doi.org/10.1175/2009JCLI2909.1.

Wilhite, D. A., 2000: Drought as a natural hazard: Concepts and definitions. *Drought: A Global Assessment*, Vol. I, D. A. Wilhite, Ed., Routledge, 3–18, http://digitalcommons.unl.edu/droughtfacpub/69.

WMO, 2021: Atlas of mortality and economic losses from weather, climate, and water extremes (1970–2019). WMO-1267, 89 pp.,

https://library.wmo.int/index.php?lvl=notice_display&id=21930#.YubOcnZBzIU.

Wu, C., P. J. F. Yeh, Y. Y. Chen, B. X. Hu, and G. Huang, 2020: Future precipitation-driven meteorological drought changes in the CMIP5 multimodel ensembles under 1.5°C and 2°C global warming. *J. Hydrometeor.*, **21**, 2177–2196, https://doi.org/10.1175/JHM-D-19-0299.1.

——, ——, ——, W. Lv, B. X. Hu, and G. Huang, 2021: Copula-based risk evaluation of global meteorological drought in the 21st century based on CMIP5 multi-model ensemble projections. *J. Hydrol.*, **598**, 126265, https://doi.org/10.1016/j.jhydrol.2021.126265.

Xu, L., N. Chen, and X. Zhang, 2019: Global drought trends under 1.5° and 2°C warming. *Int. J. Climatol.*, **39**, 2375–2385, https://doi.org/10.1002/joc.5958.

——, P. Abbaszadeh, H. Moradkhani, N. Chen, and X. Zhang, 2020: Continental drought monitoring using satellite soil moisture, data assimilation and an integrated drought index. *Remote Sens. Environ.*, **250**, 112028, https://doi.org/10.1016/j.rse.2020.112028.

Yang, X., Y. P. Li, Y. R. Liu, and P. P. Gao, 2020: A MCMC-based maximum entropy copula method for bivariate drought risk analysis of the Amu Darya River Basin. *J. Hydrol.*, **590**, 125502, https://doi.org/10.1016/j.jhydrol.2020.125502.

Zhou, T., Lu, J., Zhang, W., and Z. Chen, 2020: The sources of uncertainty in the projection of global land monsoon precipitation. *Geophys. Res. Lett.*, **47**, e2020GL088415, https://doi.org/10.1029/2020GL088415.

Zscheischler, J., and S. I. Seneviratne, 2017: Dependence of drivers affects risks associated with compound events. *Sci. Adv.*, **3**, e1700263, https://doi.org/10.1126/sciadv.1700263.